Bronisław TOMCZUK
Dawid WAJNERT
Jan ZIMON

MODELLING OF CONTROL SYSTEM FOR AN ACTIVE MAGNETIC BEARING

ABSTRACT *Active Magnetic Bearing (AMB) supports a rotor by magnetic attractive forces, without any mechanical contact. The paper presents a field-circuit model of an active magnetic bearing including its control loop. The basic parameters of the active magnetic system has been obtained from a FEM analysis of an magnetic bearing actuator. The position control system is based on operation of the local conventional PID controller, which has been widely used in industrial applications of the active magnetic bearing systems. The parameters of the controller have been obtained with the use of the root locus method. The obtained simulation and experimental results are compared in case of lifting the rotor.*

Keywords: *modelling, control system, magnetic bearing control system, Finite Element Metod, controller, simulation, rotor, levitation control algorithm, force, flux density transfer function, transmittance.*

Bronisław TOMCZUK, Prof., Ph.D, D.Sc. Eng
e-mail: b.tomczuk@po.opole.pl

Dawid WAJNERT, M.Sc, Eng.
e-mail:dawid.wajnert@op.pl

Jan ZIMON, Ph.D, Eng.
e-mail: j.zimon@po.opole.pl

Opole University of Technology

PROCEEDINGS OF ELECTROTECHNICAL INSTITUTE, Issue 252, 2011

1. INTRODUCTION

Active magnetic bearings are used in technical applications to provide the contactless levitation of the rotor. Stable operation of machines, which consist of active magnetic bearings is achieved through appropriate magnetic forces generated by the magnetic bearing actuator. Magnetic bearings have some advantages in relation to the mechanical and hydrostatic ones. The most important advantages are [9]: contactless operation and absence of lubrication and contamination wear. The rotor can be allowed to rotate at high speed, the high circumferential speed is only limited by the strength of the rotor material. At high operation speeds, friction losses are 5 to 20 times less than in the conventional ball or journal bearings. Due to the lack of mechanical wear, magnetic bearings have higher life time and lower maintenance costs. However, active magnetic bearings have also disadvantages. The design of a magnetic bearing system for a specific application requires knowledge in mechatronics, especially in mechanical and electrical engineering and in information processing. Because of the complexity of the magnetic bearing system, the costs of purchase are several times larger in relation to the conventional bearings. Though, thanks to many advantages, active magnetic bearings have found usage in many industrial applications, such as turbo-molecular vacuum pumps, flywheel energy storage systems, gas turbines, compressors, machine tools.

In this paper, the dynamic behavior of an active magnetic bearing has been analyzed. The presented dynamic model is based on the coil inductance, the velocity-induced voltage coefficient and the radial force characteristic, which are determined by the finite element method.

2. MODELLING OF THE ACTIVE MAGNETIC BEARING

2.1. Specification

The studied levitation actuator creates a 12-pole heteropolar bearing. The magnetic system has been made from laminated sheets of M270-50 silicon steel. Configuration of the 12-pole system is different from the 8-pole typical bearings. The attractive force generated in y-axis is two times greater than the force generated in the x-axis. The four control windings of the 12-pole bearing, shown in Figure 1, consists of 12 coils connected as follows: 1A-1B-1C-1D, 2A-2B, 3A-3B-3C-3D and 4A-4B. The windings 1 and 3 generate the attractive

force along the y -axis, while windings 2 and 4 generate magnetic force in the x-axis. The physical properties of the active magnetic bearing have been presented in Table 1.

TABLE 1
Specification of the radial active magnetic bearing parameters

Property	**Value**
Number of poles	12
Stator axial length	56 mm
Stator outer diameter	104 mm
Stator inner diameter	29 mm
Rotor axial length	76 mm
Rotor diameter	28 mm
Nominal air gap	1 mm
Number of turns per pole	40
Copper wire gauge	1 mm^2
Stator weight	2.6 kg
Current stiffness coefficient	13 N/A
Position stiffness coefficient	42 N/mm

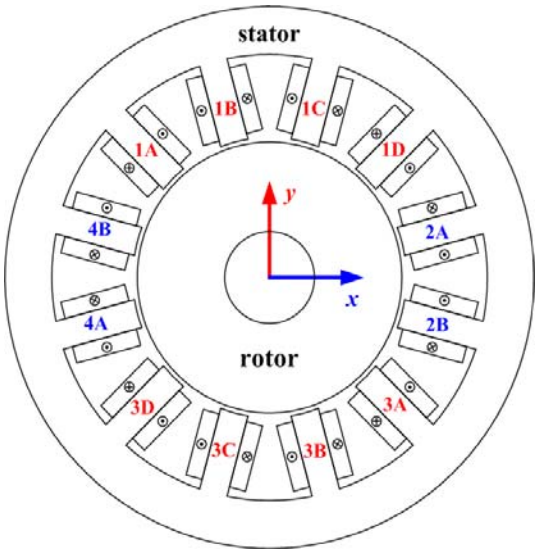

Fig. 1. Front view of the active magnetic bearing

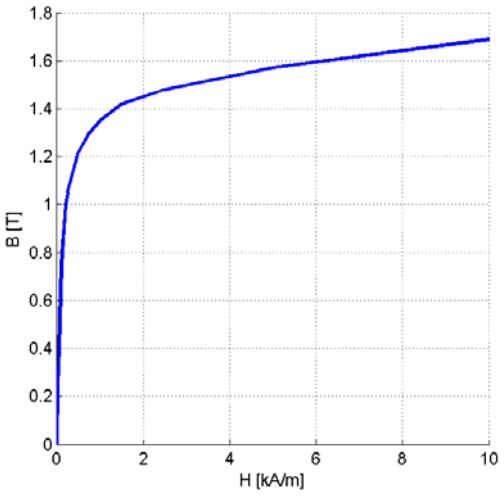

Fig. 2. B-H characteristic for the laminated ferromagnetic material M270-50

2.2. Modelling of the active magnetic bearing actuator

Active magnetic bearing is a typical electromagnetic system in which the electrical and mechanical energies are coupled by the magnetic field. A dynamic model of the active magnetic bearing in y-axis is described by the set of ordinary differential equations:

$$u_1 = R_1 i_1 + L_{d1}\frac{di_1}{dt} + h_{v1}\frac{dy}{dt}$$
$$u_3 = R_3 i_3 + L_{d3}\frac{di_3}{dt} + h_{v3}\frac{dy}{dt} \quad (1)$$

$$m\frac{d^2 y}{dt^2} = F_y(i_{cy}, y) \quad (2)$$

The voltage equations (1) determine the electrical behaviour of the active magnetic bearing, where u_1, u_3 are the supply voltages, the currents i_1, i_3 consist of bias and control ones: $i_1 = i_{by} + i_{cy}$, $i_3 = i_{by} - i_{cy}$. R_1, R_3 are the winding's resistances, L_{d1}, L_{d3} denote the dynamic inductances of the windings and h_{v1}, h_{v3} describe the velocity-induced voltage. The mechanical equations (2) determine the dynamic model of the magnetically suspended shaft.

An active magnetic bearing is characterized by the nonlinear relationship between the attractive force and position of the rotor and windings currents. Studying the opposing pair of the electromagnets the following linear relationship for the attractive force can be obtained:

$$F_y = k_{iy} i_{cy} + k_{sy} y \quad (3)$$

The current stiffness coefficient k_{iy} and position stiffness coefficient k_{sy} are defined as partial derivatives of the radial force F_y, [10]:

$$k_{iy} = \left.\frac{\partial F_y(i_{cy}, y)}{\partial i_{cy}}\right|_{y=0}, \quad k_{sy} = \left.\frac{\partial F_y(i_{cy}, y)}{\partial y}\right|_{i_{cy}=0} \quad (4)$$

The basic parameters of the active magnetic bearing actuator have been computed using FEM analysis. Simulation of the magnetic bearing was developed with Matlab/Simulink software. The block diagram of the AMB model in the y-axis for the field-circuit method is shown in Figure 3. The content of the block "Electromagnets 1 and 3" is shown in Figure 4.

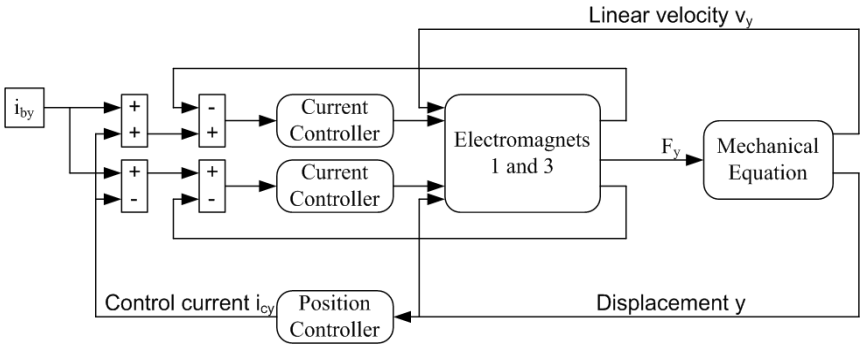

Fig. 3. Block diagram for the analysis of the AMB dynamics in *y*-axis

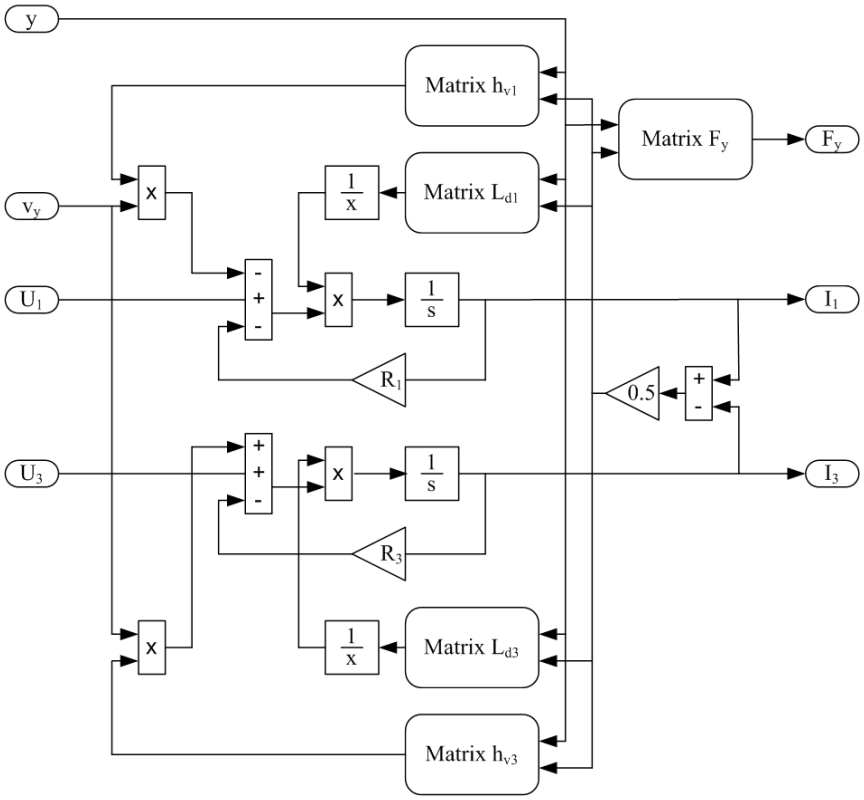

Fig. 4. The content of the block Electromagnets 1 and 3"

2.3. Finite element computation of AMB

Magnetostatic computation of magnetic field distribution in the magnetic bearing was performed by 2D Finite Element Method, using the program FEMM 4.2 [8]. The problem is formulated by Poisson's equation:

$$\nabla \times \left(\frac{1}{\mu(\vec{B})} \nabla \times \vec{A} \right) = \vec{J} \tag{5}$$

where μ is the permeability of material, $\vec{B}$ is the magnetic flux density, $\vec{A}$ is the magnetic vector potential in z direction, $\vec{J}$ is the current density. In the calcu-

lation have been included nonlinear characteristics $\mu(B)$ of the ferromagnetic material, which are shown in Figure 2. A two-dimensional model of the active magnetic bearing has been discretized by 82356 standard triangular elements (Fig. 5a). Calculation of the magnetic bearing forces by the Maxwell's stress tensor method requires a closed surface that surrounds the rotor in free space [1]. Therefore, the air gap area was divided into two subareas between stator and rotor (Fig. 5b). In order to solve equation (5) the boundary conditions have to be known. Thus, on the outer edges of the calculation area Dirichlet boundary conditions have been assumed.

a)

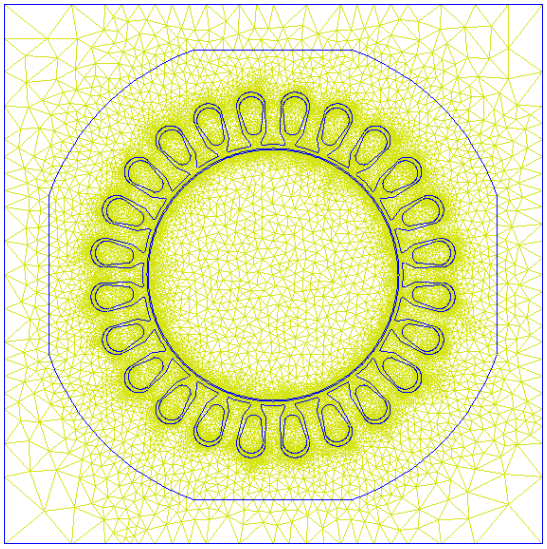

Fig. 5. Discretization of the model

b)

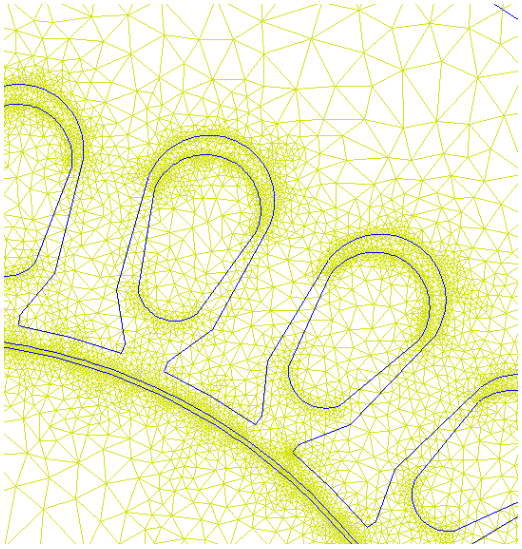

Fig. 6. The finite element mesh in the subregions of stator and rotor

As a result of equation (5) solution, the distribution of the A_z component for magnetic vector potential has been obtained. Thus, the vector of magnetic field distribution is determined as:

$$\vec{B} = \frac{\partial A_z}{\partial y} 1_x - \frac{\partial A_z}{\partial x} 1_y \tag{6}$$

Assuming the 2D field, the magnetic flux of the coils has been calculated from:

$$\Psi = \sum_{i=1}^{N} \oint_l \vec{A} \cdot d\vec{l} = \sum_{i=1}^{N} l_i \left(A_{z,i+} - A_{z,i-} \right) \tag{7}$$

where N denotes the number of turns of the coil, $A_{z,i+}$ and $A_{z,i-}$ are the vector potentials on the positive and negative sides of the coil turn, respectively.

The dynamic inductance is computed as partial derivative of the flux with respect to the current i:

$$L_d = \frac{\partial \Psi}{\partial i}, \tag{8}$$

while the velocity-induced voltage is computed as partial derivative of the flux with respect to the displacement s:

$$h_v = \frac{\partial \Psi}{\partial s} \tag{9}$$

The displacement "s" denotes "y" or "x" movement. The radial force is computed by Maxwell's stress tensor method, in which the electromagnetic force is obtained as surface integral:

$$F = \frac{1}{2}\oint_S \left\{\vec{H}(\vec{n}\cdot\vec{B}) + \vec{B}(\vec{n}\cdot\vec{H}) - \vec{n}(\vec{H}\cdot\vec{B})\right\} d\vec{s} \tag{10}$$

where $\vec{H}$ is the magnetic field intensity and $\vec{n}$ is the unit surface normal to $\vec{S}$.

The flux density plot for control current i_{cy} = 4 A, i_{cx} = 0 A and at the central position of the rotor (x = y = 0 mm) is presented in Figure 7. For that condition, the active magnetic bearing generates maximum radial force in the y-axis, whereas the component in x-axis is equal zero. An average value of the flux density in the pole tooth is 1.30 T.

a) b)

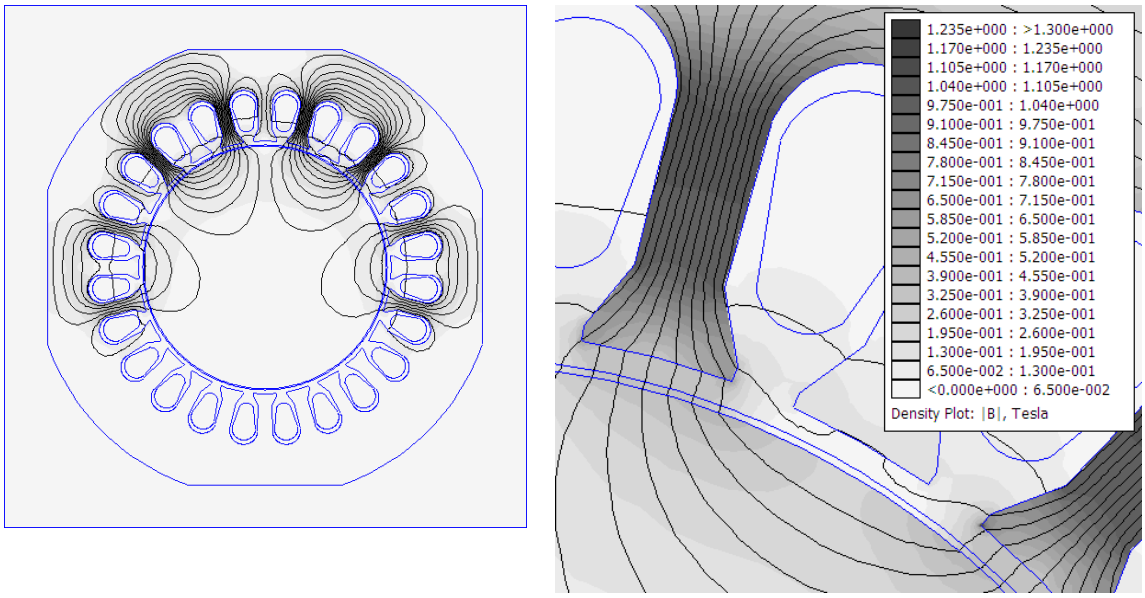

Fig. 7. Magnetic field distribution for the case i_b = 4 A, i_{cy} = 4 A, i_{cx} = 0 A and x = y = 0 mm in whole geometry of active magnetic bearing (a) and in the pole teeth (b)

The radial force characteristic F_y and fluxes Ψ_1, Ψ_3 in the coils have been calculated over the entire operating range $i_{cy}\in$(-4.0 A, 4.0 A), $y\in$(-0.3 mm, 0.3 mm). The radial force F_y and flux Ψ_1 characteristics are presented in Figure 8 and Figure 9.

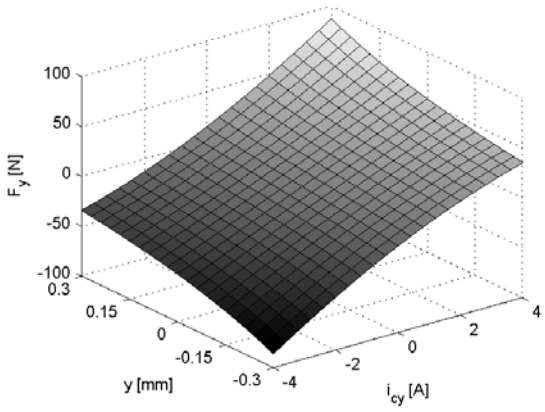

Fig. 8. Radial force characteristic $F_y(i_{cy},y)$

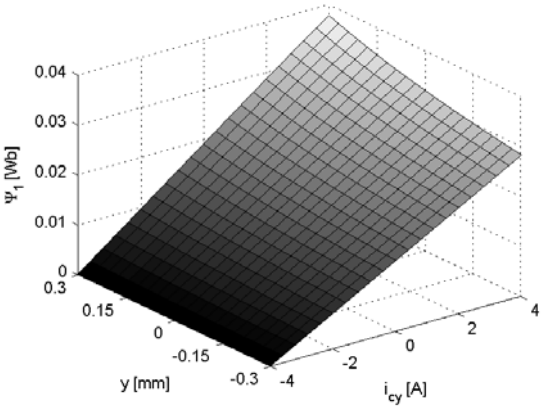

Fig. 9. Flux characteristic $\Psi_1(i_{cy},y)$

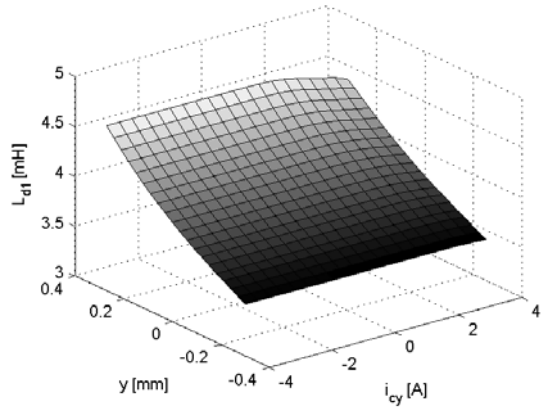

Fig. 10. Dynamic inductance characteristic $L_{d1}(i_{cy},y)$

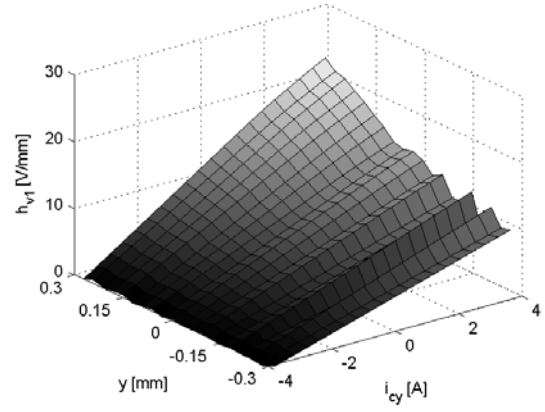

Fig. 11. The velocity-induced voltage characteristic $h_{v1}(i_{cy},y)$

2.4. Control system for the Active Magnetic Bearing

In recent years there have been developed and implemented various algorithms to control the active magnetic bearings. The most important ones are: PID control [4], gain scheduled control [2], robust H_∞ control [6], LQ control [11], fuzzy logic control [5], feedback linearization control [7]. Despite of intensive development of the advanced control algorithms for the active

magnetic bearing, the industrial applications of the magnetic bearing were mostly based on analog or digital PID controllers.

The transformation function of the current controlled active magnetic bearing in y-axis is expressed by the following equation:

$$G_{AMB}(s) = \frac{k_{iy}}{ms^2 - k_{sy}} \tag{11}$$

The poles of the transfer function describe an unstable system, because one of the poles has a positive value. Thus, the active magnetic bearing requires a control system. Stable operation can be obtained with decentralized PID controller, with the transfer function [3]:

$$G_{PID}(s) = K_P + \frac{K_I}{s} + sK_D \tag{12}$$

The block diagram of the control system with PID controller for y-axis is shown in Figure 12, where $y_r(t)$ is the reference value of the rotor position (generally equal to zero), $i_{cy}(t)$ is the reference control current and $y(t)$ is position of the rotor.

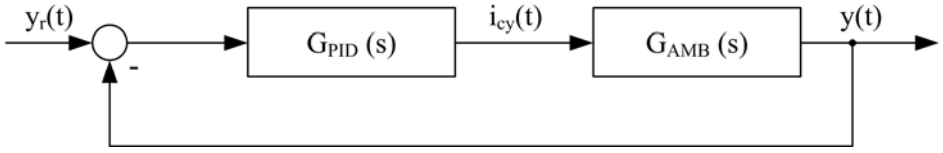

Fig. 12. Block diagram of the control system

Laplace transfer function of the closed loop is described by the transmittance:

$$G_{CL}(s) = \frac{\frac{K_D k_{iy}}{m}s^2 + \frac{K_P k_{iy}}{m}s + \frac{K_I k_{iy}}{m}}{s^3 + \frac{K_D k_{iy}}{m}s^2 + \frac{K_P k_{iy} - k_{sy}}{m}s + \frac{K_I k_{iy}}{m}} \tag{13}$$

The closed-loop system with the PID controller has three poles λ_1, λ_2, λ_3. To determine the value of K_P, K_I, K_D, the coef/ficients of the denominator of $G_{CL}(s)$ in Eq. 13 should be compared with the coefficients of the polynomial form:

$$s^3 + (\lambda_1 + \lambda_2 + \lambda_3)s^2 + (\lambda_1\lambda_2 + \lambda_2\lambda_3 + \lambda_1\lambda_3)s + \lambda_1\lambda_2\lambda_3 \tag{14}$$

Thus, the parameters of the PID controller are equal to:

$$K_P = \frac{(\lambda_1\lambda_2 + \lambda_2\lambda_3 + \lambda_3\lambda_1)m + k_{sy}}{k_{iy}}$$
$$K_I = \frac{-\lambda_1\lambda_2\lambda_3 m}{k_{iy}} \tag{15}$$
$$K_D = \frac{(-\lambda_1 - \lambda_2 - \lambda_3)m}{k_{iy}}$$

Location of the poles λ_1, λ_2, λ_3 in the s-plane affects the nature of the transients. According to the pole placement method [4] two poles can be determined from:

$$\lambda_1 = -\omega_n\zeta + i\omega_n\sqrt{1-\zeta^2}$$
$$\lambda_2 = -\omega_n\zeta - i\omega_n\sqrt{1-\zeta^2} \tag{16}$$

where ω_n is the undamped natural frequency:

$$\omega_n = \frac{4.6}{t_s\zeta} \tag{17}$$

The third pole of transfer function of $G_{CL}(s)$ should be located outside the dominant area. Thus, the coefficients K_P, K_I, K_D depend on the settling time t_S and damping ratio ζ.

3. SIMULATION AND EXPERIMENTAL RESULTS

For the rotor stabilization two decoupled PID controllers were used. The control tasks have been realized with 32-bit microcontroller with very efficient ARM7TDMI-S core. The sampling frequency of PID controllers are equal to 1 kHz. The position of the rotor is measured by Turck contact-less inductive sensor with bandwidth 200 Hz. The analog to digital converters resolution equals 2.44 μm. The parameters of PID controllers were determined according to the proposed method for the settling time t_S = 50 ms and the damping coefficient ζ = 0.5. The values of parameters of PID controllers are shown in Table 2.

TABLE 2
Parameters of the PID controller

KP [A/m]	KI [A/ms]	KD [As/m]
11231	514080	45

Figures 13 and 14 present the comparison of simulated and experimental results during rotor lifting. The curve characters of the characteristics are close to the measured ones. It can be seen that the current value in the steady state is slightly higher in the real system.

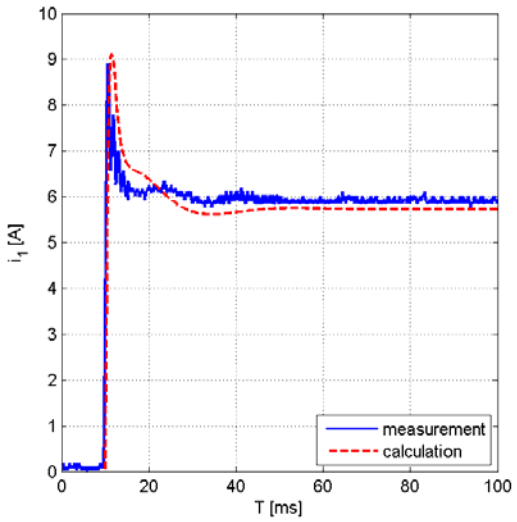

Fig. 13. Time response of current i_1

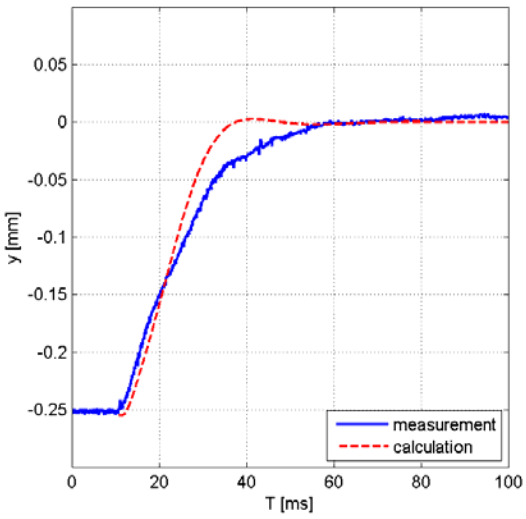

Fig. 14. Time response of the AMB shaft displacement in y-axis

The transient state for the rotor position for both systems differs, also because the settling time in the simulated system is shorter than in the real one. Differences are due to the simplified modelling of the magnetic bearing's actuator, especially because of disregarding the hysteresis phenomena and the fringing effect.

4. REMARKS AND CONCLUSION

This work presents a method for modelling control systems for active magnetic bearings. The dynamic behavior of active magnetic bearings has been obtained from a field-circuit model. The basic parameters of the active magnetic bearing actuator have been computed using FEM analysis .

The presented method for designing PID controllers makes the tuning of the controller parameters easier and assures a good damping.

LITERATURE

1. Antila M., Lantto E., Arkkio A.: Determination of Forces and Linearized Parameters of Radial Active Magnetic Bearings by Finite Element Technique, IEEE Transaction On Magnetics, Vol. 34, No. 3, 1998, pp. 684-694.
2. Betschon F., Knospe C.R.: Reducing magnetic bearing currents via gain scheduled adaptive control, IEEE/ASME Transactions on Mechatronics, Vol. 6, No. 4, 12.2001, pp. 437-443.
3. FranklinG.: Feedback control of dynamic systems, Prentice Hall, New Jersey, 2002.
4. Gosiewski Z., Falkowski K.: Wielofunkcyjne łożyska magnetyczne, Biblioteka Naukowa Instytutu Lotnictwa, Warszawa, 2003.
5. Hung. J.Y.: Magnetic bearing control using fuzzy logic, IEEE Transactions on Industry Applications, Vol. 31, No. 6, 11.1995, pp. 1492-1497.
6. Lantto E.: Robust Control of Magnetic Bearings in Subcritical Machines, PhD thesis, Espoo, 1999.
7. Lindlau J., Knospe C.: Feedback Linearization of an Active Magnetic Bearing With Voltage Control, IEEE Transactions on Control Systems Technology, Vol. 10, No.1, 01.2002, pp. 21-31.
8. Meeker D.: Finite Element Method Magnetics Version 4.2, User's Manual, University of Virginia, U.S.A, 2009.
9. Schweitzer G., Maslen E.: Magnetic Bearings, Theory, Design and Application to Rotating Machinery, Springer, Berlin, 2009.
10. Tomczuk B., Zimon J.: Filed Determination and Calculation of Stiffness Parameters in an Active Magnetic Bearing (AMB), Solid State Phenomena, Vol. 147-149, 2009, pp. 125-130.
11. Zhuravlyov Y.N.: On LQ-control of magnetic bearing, IEEE Transactions On Control Systems Technology, Vol. 8, No. 2, 03.2000, pp. 344-355.

Manuscript submitted 08.07.2011

MODELOWANIE SYSTEMU STEROWANIA DLA AKTYWNEGO ŁOŻYSKA MAGNETYCZNEGO

Bronisław TOMCZUK,
Dawid WAJNERT, Jan ZIMON

STRESZCZENIE *Aktywne łożysko magnetyczne podtrzymuje wirnik magnetycznymi siłami przyciągania, bez kontaktu mechanicznego. Przedstawiono model obwodów magnetycznych aktywnego łożyska magnetycznego włącznie z jego pętla sterowania. Podstawowe*

parametry aktywnego układu magnetycznego otrzymano z analizy FEM (metoda elementów skończonych) aktuatora łożyska magnetycznego. System sterowania położeniem oparty jest na działaniu lokalnego konwencjonalnego sterownika PID, który był szeroko stosowany w przemysłowych zastosowaniach systemów z aktywnymi łożyskami magnetycznymi. Parametry sterownika otrzymano metodą miejsca geometrycznego pierwiastków (równania charakterystycznego układu). Otrzymana symulacja i wyniki doświadczalne są porównane dla przypadku lewitacji wirnika.

KAPITAŁ LUDZKI
NARODOWA STRATEGIA SPÓJNOŚCI

UNIA EUROPEJSKA
EUROPEJSKI
FUNDUSZ SPOŁECZNY

Work co-financed by European Social Fund